Photon production from Pb + Pb collisions at $\sqrt{s_{NN}} = 5.02$ TeV at the CERN Large Hadron Collider and at $\sqrt{s_{NN}} = 39$ TeV at the proposed Future Circular Collider facility

Pingal Dasgupta,[1,2,*] Somnath De,[3,†] Rupa Chatterjee,[1,2,‡] and Dinesh K. Srivastava[1,2,4,5,§]

[1]*Variable Energy Cyclotron Centre, HBNI, 1/AF, Bidhan Nagar, Kolkata-700064, India*

[2]*Homi Bhabha National Institute, Training School Complex, Anushakti Nagar, Mumbai 400085, India*

[3]*Pingla Thana Mahavidyalaya under Vidyasagar University, West Bengal-721140, India*

[4]*Institut für Theoretische Physik, Johann Wolfgang Goethe-Universität, Max-von-Laue-Str. 1, D-60438 Frankfurt am Main, Germany*

[5]*ExtreMe Matter Institute EMMI, GSI Helmholtzzentrum für Schwerionenforschung, Planckstrasse 1, 64291 Darmstadt, Germany*

(Received 11 April 2018; revised manuscript received 14 June 2018; published 16 August 2018)

We calculate the production of prompt and thermal photons from Pb + Pb collisions at 5.02A TeV at the Large Hadron Collider (LHC) and at 39A TeV at the proposed Future Circular Collider (FCC) facility. The photon spectra and anisotropic flow at these energies are compared with the results obtained from 2.76A TeV Pb + Pb collisions at the LHC for three different centrality bins. The prompt photons originating from initial hard scatterings are found to increase by a factor of 1.5 to 2 at 5.02A TeV in the p_T region 2 to 15 GeV and the enhancement is found to be about 5 to 15 times at FCC energies compared with 2.76A TeV in the same p_T region. The evolution of the quark-gluon plasma (QGP) formed in Pb + Pb collisions at LHC and FCC energies are studied by using a hydrodynamical model and the p_T spectra and elliptic flow of thermal photons are calculated using state-of-the-art photon rates. The relative enhancement in the production of thermal photons is found to be more compared with prompt photons at FCC than at the LHC energies. Although the production of direct (prompt + thermal) photons is found to enhance significantly with increase in beam energy, the photon elliptic flow increases only marginally and does not show strong sensitivity to the collision energy.

DOI: 10.1103/PhysRevC.98.024911

I. INTRODUCTION

Experiments performed at the Relativistic Heavy Ion Collider (RHIC) and at the Large Hadron Collider (LHC) are aimed at exploring a specific region of the QCD phase diagram where a possible transition from a bound state of hadrons to an unbound state of quarks and gluons can occur. This color-deconfined state of quarks and gluons in local thermal equilibrium is known as a quark-gluon plasma [1,2]. Relativistic hydrodynamics has emerged as one of the most successful frameworks to explain the soft probes or bulk observables produced in high-energy heavy-ion collisions [3,4]. The charged particle spectra as well as anisotropic flow parameters (elliptic, triangular flow, etc.) are successfully explained by hydrodynamic model with suitable initial conditions where the initial conditions are constrained from the experimental data for final charged particle multiplicity [5–8].

Photons, both real as well as virtual (i.e., dileptons), are known as one of the promising probes to study the hot and dense quark-gluon plasma produced in relativistic heavy-ion collisions [9,10]. The direct photon spectra at 200A GeV Au + Au collisions at RHIC and at 2.76A TeV Pb + Pb collisions at the LHC are explained well in the region $p_T > 1$ GeV by a calculation combining the contributions of prompt and thermal photons where the prompt photons are calculated by using a next-to-leading order (NLO) perturbative QCD calculation and the thermal part is calculated considering a hydrodynamic evolution of the fireball produced and state-of-the-art photon production rates [11–14]. However, the very low p_T ($\leqslant 1$ GeV) region of the direct photon spectra which is likely to be dominated by photons produced from the interaction of different hadronic channels still remains unexplained by most of the calculations. Most importantly, it has been shown in many recent studies that the calculations underpredict the experimental data on the elliptic and triangular flow of photons by a large margin both for Au + Au collisions at the RHIC and Pb + Pb collisions at the LHC [11,12,15]. Thus, model calculations that simultaneously explain the spectra and anisotropic flow of charged particles from heavy-ion collisions fail to reproduce the photon spectra and anisotropic flow parameters at RHIC [16,17] and LHC energies [18,19]. This is known as the *photon v_2 puzzle*. The calculation of photon anisotropic flow parameter at higher collision energies, at different collisions centralities as well as for different systems (e.g., Cu + Cu, U + U) with modified initial conditions would be valuable to understand this puzzle [15,20,21].

In the past few years, direct photon production in relativistic heavy-ion collisions has emerged as a rich field of activities and some notable contributions can be found in Refs. [22–34]. Photon emission during the pre-equilibrium era of relativistic

*pingaldg@vecc.gov.in
†somvecc@gmail.com
‡rupa@vecc.gov.in
§dinesh@vecc.gov.in

heavy-ion collisions was first addressed in Ref. [35]. This source of photons contains valuable information about reaction dynamics of partons which are thermalized to QGP. In recent times, several groups have discussed the pre-equilibrium emission of photons and found that the contribution is significant in the low-p_T region of direct photon spectrum [36,37]. The strongly coupled gauge theories ($N = 4$, supersymmetric Yang–Mills) are widely applied nowadays in order to understand different phenomena of nonperturbative QCD. Thermal photon and dilepton production at finite temperature are calculated from these theories and can be found in Refs. [38–40].

Note that the initial parameters which play a significant role in hydrodynamic model calculations, the formation time, initial temperature, freeze-out temperature, etc. are not known precisely to date. We also know that the photon spectra are much more sensitive to the initial state of the produced fireball than the hadron spectra because the hadrons are only emitted from the freeze-out surface, whereas photons are emitted throughout the system evolution [41,42]. Thus, we calculate the production and anisotropic flow of direct photons at $\sqrt{s_{NN}} = 5.02$ TeV, the highest energy for Pb + Pb collisions achieved at LHC to date. We expect that Pb + Pb collisions at 5.02A TeV would be quite valuable to constrain the initial conditions as well as helpful to understand the discrepancy between the theory calculation and experimental data on photon elliptic flow parameter. The inverse slope of the photon spectra at 5.02A TeV would provide the effective temperature of the produced QGP matter at that energy. In this study we estimate the production of prompt photons at 5.02A TeV Pb + Pb collisions for three different centrality bins and compare those with the photon results obtained from 2.76A TeV Pb + Pb collisions at the LHC. In addition, we calculate the production and elliptic flow of thermal photons at 5.02A TeV for different centrality bins.

The proposed Future Circular Collider (FCC) aims to collide protons at 100 TeV. Heavy-ion collision at FCC energy is a part of accelerator design study [43–45]. The Pb + Pb collisions at FCC are expected to happen at 39A TeV, which is more than seven times larger than the top LHC energy achieved for Pb + Pb collisions to date. Predictions from hydrodynamic model calculation have shown that the charged particle multiplicity, lifetime, and volume of the produced fireball (for most-central Pb + Pb collisions) would increase by a significantly large factor at FCC compared with LHC energies [45]. One can also expect to see a large enhancement in the production of direct photons at the FCC compared with the LHC. We have seen a marginal enhancement in the photon elliptic flow at the LHC compared with the RHIC. Thus, the estimation of photon v_2 at the FCC would be valuable to determine how sensitive the anisotropic flow parameter is to the beam energy of heavy-ion collisions. In addition, the significant enhancement in photon production at the FCC is also expected to reduce the large error bars in the experimental photon v_2 data, and this would be helpful in understanding the discrepancy between the experimental data and results from calculations.

We predict the production of direct photons (prompt and thermal) from Pb + Pb collisions at 39A TeV at the FCC and compare with the results obtained at the two (2.76A and 5.02A TeV) LHC energies. The elliptic flow parameter calculated at the FCC would provide an upper limit of the photon v_2 which can be achieved in heavy-ion collisions. We shall see that the prompt photons and thermal photons as well as the elliptic flow of thermal photons change by differing extents as the energy of the collisions and the resulting initial conditions are changed. Thus an accurate description of the direct photon (sum of the thermal and prompt) spectrum along with the elliptic flow can constrain our description for these.

The paper is organized as follows: We discus the production of prompt photons in Sec. II. The hydrodynamics model and thermal photon calculations are discussed in Sec. III. In Sec. IV we show the results of photon spectra and elliptic flow parameter. The summary and conclusions are given in Sec. V.

II. PROMPT PHOTONS

Prompt photons, which are produced from initial hard scatterings of the colliding nucleons, are the dominant source of direct photons in the high-p_T region ($p_T \geqslant 4$ GeV). Quark-gluon Compton scattering [$q\ (\bar{q}) + g \longrightarrow q\ (\bar{q}) + \gamma$], quark-antiquark annihilation ($q + \bar{q} \longrightarrow g + \gamma$), and bremsstrahlung emission from final-state partons [$q(\bar{q}) \longrightarrow q(\bar{q}) + \gamma$] are the leading production channels of prompt photons. The photons emitted in the first two reactions are known as *direct* prompt photons and those emitted from the bremsstrahlung process are known as *fragmentation* photons. The prompt-photon production cross section in elementary hadron-hadron ($A + B$) collisions can be expressed as [46]

$$\frac{d^2\sigma^\gamma}{d^2p_T dy} = \sum_{i,j} \int dx_1 f_A^i(x_1, Q_f^2) \int dx_2 f_B^j(x_2, Q_f^2) \times \sum_{c=\gamma,q,g} \int \frac{dz}{z^2} \frac{d\sigma_{ij\to cX}(x_1, x_2; Q_R^2)}{d^2p_T^c dy_c} D_{c/\gamma}(z, Q_F^2), \tag{1}$$

where $f_A^i(x_1, Q_f^2)$ is the parton distribution function (PDF) of the ith (flavored) parton in hadron A carrying a momentum fraction x_1. Similarly, $f_B^j(x_2, Q_f^2)$ corresponds to the PDF for the jth (flavored) parton in hadron B carrying a momentum fraction x_2. Q_f is the factorization scale appearing from the QCD factorization scheme [47,48]. $D_{c/\gamma}(z, Q_F^2)$ denotes the parton-to-photon vacuum fragmentation probability defined at $z = p_\gamma/p_c$ and Q_F is the fragmentation scale also appearing under the same QCD factorization scheme. The fragmentation function reduces to $\delta(1 - z)$ when a photon is emitted in the direct process, i.e., $c = \gamma$. The term $\sigma_{ij\to cX}(x_1, x_2; Q_R^2)$ signifies the hard parton-parton cross section for all the relevant processes in which a photon is produced either directly or fragmented off the final-state partons (q or g). Q_R is the momentum scale which appears due to the renormalization of the running coupling constant $\alpha_s(Q^2)$.

For the nucleus-nucleus ($A + A$) collisions we replace the elementary nucleon PDF [see Eq. (1)] by the isospin-averaged nuclear PDF:

$$f_A^i(x, Q^2) = R_A(x, Q^2)\left[\frac{Z}{A} f_p^i(x, Q^2) + \frac{A - Z}{A} f_n^i(x, Q^2)\right], \tag{2}$$

where $R_A(x, Q^2)$ is the nuclear modification to the PDF [49] and f_p^i, f_n^i are the free proton and neutron PDFs, respectively. We have used the EPS09 parametrization [50] of the nuclear shadowing function in this study. Z and A are the atomic number and atomic mass respectively of the colliding nucleus. For a noncentral collision at impact parameter b we replace Z and A by the effective atomic and mass number, respectively, by using the relation [51]

$$Z_{\rm eff} = \frac{Z}{A}\frac{N_{\rm part}(b)}{2}, \quad N_{\rm eff} = \frac{N}{A}\frac{N_{\rm part}(b)}{2}. \tag{3}$$

Here, $N_{\rm part}(b)$ is the number of participant (or wounded) nucleons in an $A + A$ collision at impact parameter b calculated by using Glauber model formalism. The prompt-photon invariant yield is obtained from the differential production cross section in nucleon-nucleon (nn) collisions as

$$\frac{d^2N_{\rm AA}^{\gamma}}{d^2p_T dy} = \frac{d^2\sigma_{nn}^{\gamma}}{d^2p_T dy} T_{\rm AA}(b), \tag{4}$$

where $T_{\rm AA}(b)$ is the nuclear overlap function.

In the present study, we estimate the prompt-photon production from Pb + Pb collisions at midrapidity ($|y| < 0.5$) by using the CTEQ6.6 parton distribution functions [52] and BFG-II photon fragmentation functions [53]. We have used the Monte Carlo code JETPHOX (version 1.2.2) [54], which includes all leading-order and the next-to-leading order (in α_s) channels of prompt-photon production [55]. We consider Q_R, Q_f, and Q_F to be same ($=Q$) and all equal to the p_T of photons. One can fine tune these scales to reproduce the experimental prompt-photon spectra in $p + p$ collisions. It has been shown in Ref. [56] that calculation considering a scale value of $p_T/2$ agrees well with the experimental data from 200 GeV $p + p$ collisions at the RHIC. However, at 2.76 TeV at the LHC, the data match with the result from theoretical calculations for a scale value of p_T of the produced photons [57]. In the absence of any better guideline for choosing these scales at the higher LHC energies or the FCC energies, we have chosen the same scale, i.e., $Q = p_T$ for these energies as well.

III. HYDRODYNAMIC FRAMEWORK AND INITIAL CONDITIONS

We have considered a longitudinally boost-invariant (2 + 1)-dimensional ideal hydrodynamic framework [58] with a smooth initial density distribution to study the evolution of the hot and dense fireball produced in Pb + Pb collisions at relativistic energies. It has been shown in earlier studies that the effect of fluctuations is found to be less pronounced for heavy-ion collisions at 2.76A TeV than at 200A GeV [42]. In addition, event-by-event fluctuating initial conditions are found to affect the anisotropic flow of photons significantly more for Cu + Cu collisions compared with Au + Au collisions at the RHIC [15]. As a result, the effect of initial-state fluctuation on the thermal-photon production and its anisotropic flow is expected to be less significant at 5.02A TeV and at 39A TeV than at 2.76A TeV Pb + Pb collisions at the LHC. However, a calculation considering the event-by-event fluctuating initial conditions would be valuable to get a precise estimate of the production of direct photons at these very high energies, and we postpone that for a future study. In our calculation, an entropy initialized smooth transverse profile is constructed by taking average over a sufficiently large number of Monte Carlo (MC) events as follows [21]:

$$s(x, y) = \frac{1}{N}\sum_{j=1}^{N} s_j(x, y), \tag{5}$$

where $s_j(x, y)$ denotes the transverse entropy density profile for a single MC event. For simplicity we consider a wounded nucleon (WN) profile and the initial entropy density is distributed in the transverse plane by using the relation

$$s_j(x, y) = K\sum_{i=1}^{N_{\rm wn}} f_i(x, y), \tag{6}$$

where $N_{\rm wn}$ is the total number of wounded nucleons in an event, K is a constant factor that is tuned from the final charged particle multiplicity, and $f_i(x, y)$ is a two-dimensional Gaussian distribution function of the form

$$f_i(x, y) = \frac{1}{2\pi\sigma^2}\exp\left(-\frac{(x - x_i)^2 + (y - y_i)^2}{2\sigma^2}\right), \tag{7}$$

where (x_i, y_i) is the position of the ith source in the transverse plane. The parameter σ decides the size of the initial density fluctuation and we use $\sigma = 0.4$ fm for our calculations [58,59].

We take the inelastic nucleon-nucleon cross section ($\sigma_{\rm NN}$) as 64, 70, and 80 mb at the beam energies 2.76A, 5.02A, and 39A TeV, respectively [12,45]. The final charged-particle multiplicity ($dN_{\rm ch}/d\eta$) for 0%–5% centrality class from which the overall normalization constant [K in Eq. (6)] is fixed, is taken as 2000 at 5.20A TeV and 1600 at 2.76A TeV Pb + Pb collisions at the LHC from the experimental data. For the FCC, the final charged particle multiplicity for most-central collisions is estimated by extrapolating the results at RHIC and LHC energies by using the relation $dN_{\rm ch}/d\eta \propto (\sqrt{s_{NN}})^{0.3}$. We get ($dN_{\rm ch}/d\eta$) as 3600 at the FCC, which can be considered as an upper limit of the charged-particle multiplicity [45].

The initial thermalization time of the hydrodynamic evolution is taken as $\tau_0 = 0.14$ fm/c for 2.76A TeV collisions [12] and we retain the same value for τ_0 even for the higher beam energies considered in the present study. One may argue that the system would take less time to thermalize for higher beam energies. However, we believe that this value of τ_0 is already too small and, in addition, at present we do not have any result from theoretical calculations predicting the formation time at 5.02A and 39A TeV. Thus, $\tau_0 = 0.14$ fm/c can be considered as a good approximation of τ_0 for all three energies. The temperature at freeze-out (T_f) is taken as 160 MeV, which reproduces the measured p_T spectra of charged pions at 2.76A TeV at the LHC energy. The quark-hadron transition temperature T_c is taken as 170 MeV and the lattice-QCD-based equation of state is taken from Ref. [60]. We choose centrality cuts in our calculation by using the MC Glauber model.

It is important to mention here that a two-component (combination of wounded nucleons and binary collisions) Glauber model initial condition is more effective (than a wounded nucleon profile) for very high energy $A + A$ collisions where

we fix the fraction of the two components from the charged-particle multiplicity distribution. However, at FCC energy, as there is no experimental data available, we consider a single-component Glauber model to estimate the thermal-photon production at different centralities to avoid introducing an additional parameter.

IV. THERMAL PHOTONS

We use next-to-leading-order plasma rates from Refs. [61,62] to calculate the photon production from the QGP phase. The rates for photon production from the hadronic phase (an exhaustive set of hadronic reactions and radiative decay of higher resonance states are considered) have been taken from Ref. [63] and which also include the effects of the hadronic form factors. The p_T spectrum of thermal photons is obtained by integrating the emission rates ($R = EdN/d^3pd^4x$) over the entire spacetime history. The evolution is considered from the initial thermalization time to the final freeze-out state of the fireball via the intermediary quark-hadron transition:

$$E\frac{dN}{d^3p} = \int d^4x R(E^*(x), T(x)), \tag{8}$$

where $T(x)$ is the local temperature. The energy in the comoving frame is $E^*(x) = p^\mu u_\mu(x)$, where p^μ is the four-momentum of the photons and u_μ is the local four-velocity of the flow field. The values of T and u_μ are obtained by solving the hydrodynamical equations.

The anisotropic flow coefficients v_n are estimated by expanding the invariant particle distribution in transverse plane by using a Fourier decomposition:

$$\frac{dN}{d^2p_T dy} = \frac{1}{2\pi}\frac{dN}{p_T dp_T dy}\left[1 + 2\sum_{n=1}^{\infty} v_n(p_T)\cos(n\phi)\right]. \tag{9}$$

For a smooth initial density distribution the first nonvanishing anisotropic flow coefficient is v_2 or the elliptic flow parameter.

V. RESULTS

A. Prompt-photon production

The prompt-photon spectra from Pb + Pb collisions at 5.02A TeV at the LHC and 39A TeV at the FCC for centrality bins 0%–20%, 20%–40%, and 40%–60% are shown in Fig. 1. The results from 2.76A TeV are also shown in the same figures for a comparison. For 0%–20% centrality bin one can see that, in the p_T range 2–15 GeV, the production of prompt photons is about 1.5–2 times larger at 5.02A TeV compared with 2.76A TeV. We see a much larger production of prompt photons at the FCC compared with the LHC; at $p_T \sim 2$ GeV the spectra (for all three centrality bins) at the FCC is about five times larger than at 2.76A TeV. As we move towards higher p_T values, the enhancement in the production at the FCC compared with the LHC is even more. At $p_T \sim 15$ GeV, the enhancement factor is about 15 for prompt photons at 39A TeV than at 2.76A TeV. However, the difference between spectra at the two LHC energies remains almost the same in the entire p_T range shown in the figure. Prompt-photon yield for 0%–20%

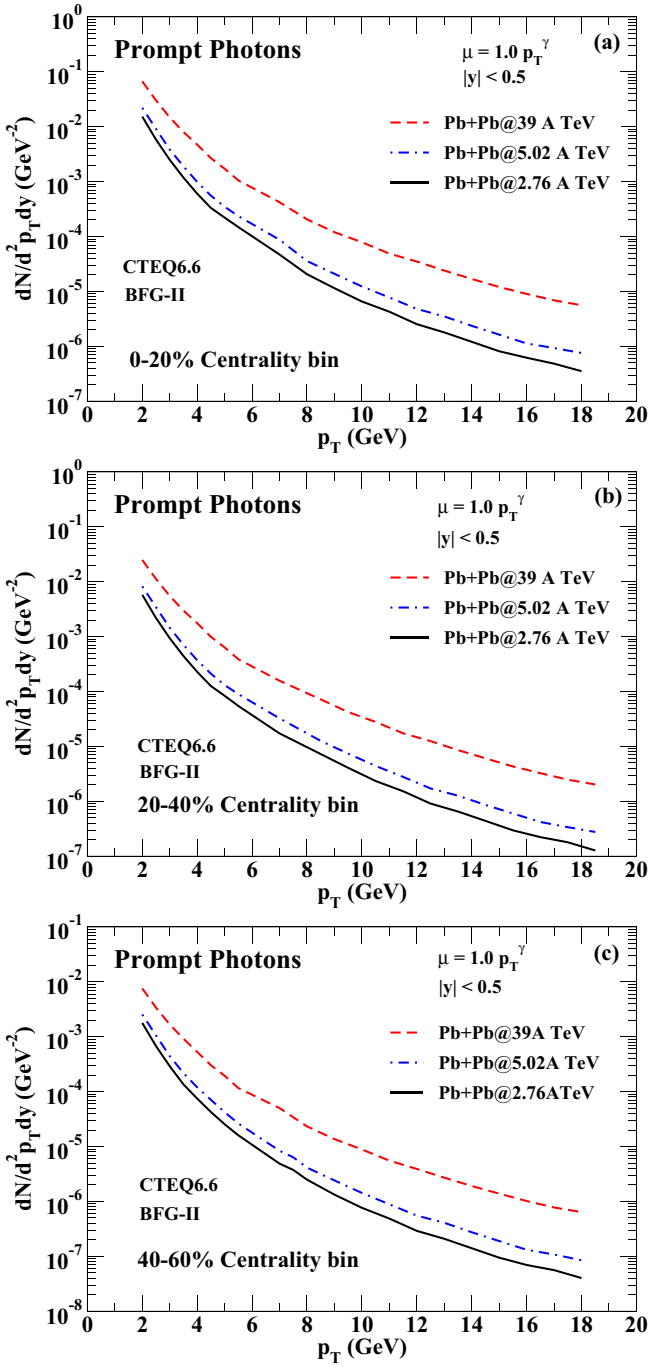

FIG. 1. Prompt-photon spectra from Pb + Pb collision at 2.76A and 5.02A TeV at LHC and at 39A TeV at FCC for centrality bins (a) 0%–20%, (b) 20%–40%, and (c) 40%–60%.

central collisions is found to be almost nine to ten times larger than the same obtained for 40%–60% centrality and almost three to four times larger for 20%–40% collision centralities for all beam energies. However, the relative enhancement in the production at the three collision energies is found to be similar for all three centrality bins. These variations are well beyond that due to the variation in the number of collisions ($N_{\rm coll}$).

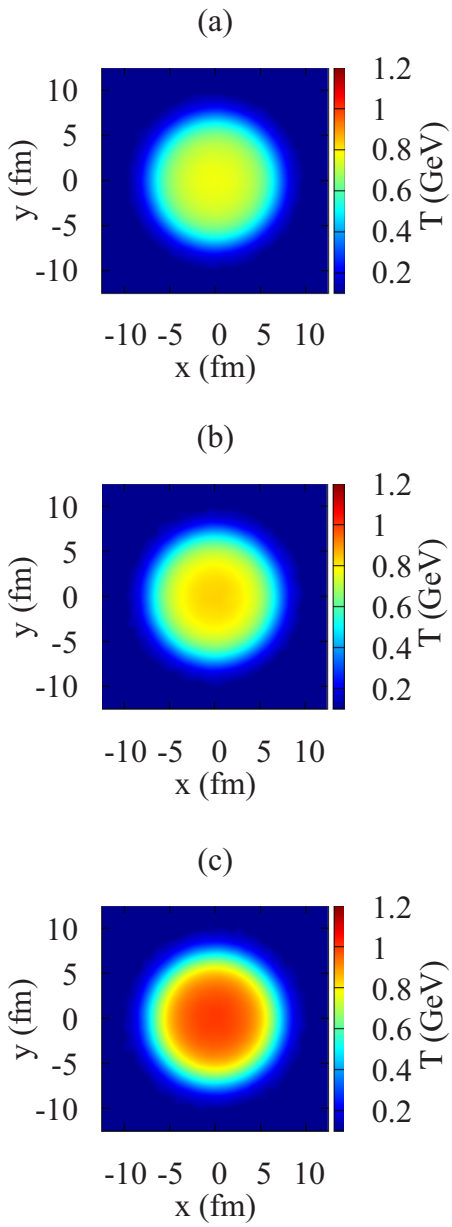

FIG. 2. Distribution of temperature at formation time τ_0 (taken as 0.14 fm/c) on transverse (x-y) plane for central ($b \approx 0$ fm) Pb + Pb collisions at (a) 2.76A TeV and (b) 5.02A TeV at the LHC and (c) at 39A TeV at the FCC. Color bars give the index of temperature in GeV.

B. Hydrodynamic evolution of hot and dense matter produced at Large Hadron Collider and Future Circular Collider energies

The distribution of the initial temperature on the transverse plane for the most-central ($b \approx 0$) collision of Pb nuclei at 2.76A, 5.02A, and 39A TeV is shown in Fig. 2. The value of τ_0 is taken as 0.14 fm/c (as discussed earlier) for all three cases. The smooth initial temperature distribution as shown in the figure is obtained by averaging over 10 000 events with fluctuating initial density distributions [using Eq. (5)]. Color bars shown alongside the figure indicate the temperature values. The temperature profile at 5.02A TeV looks hotter

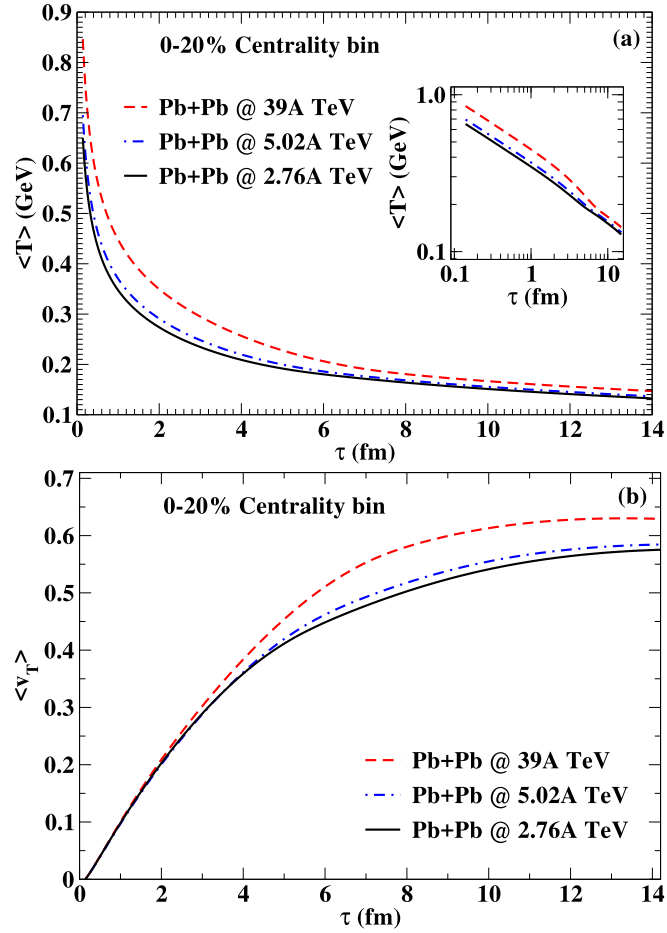

FIG. 3. Time evolution of (a) average temperature and (b) average transverse flow velocity from 0%–20% central collisions of Pb + Pb at 39A, 5.02A, and 2.76A TeV.

than the profile at 2.76A TeV, as expected, while at the FCC energy the central region shows significantly larger temperature compared with both the LHC energies. At the FCC, the central temperature (at $x = y = 0$) is found to be more than 1 GeV, which is significantly larger than the maximum central temperatures at the LHC energies. Hence, more prominent QGP signatures are expected to be obtained from the hotter and longer-lived QGP phase at the FCC compared with the LHC energies. The time evolution of average temperature and average transverse flow velocity for the three energies (at centrality bin 0%–20%) are shown in Fig. 3. The averages of the thermodynamic quantities are calculated by using Eq. (8) of Ref. [21]. The $\langle T \rangle$ at the FCC is about 850 MeV, whereas it is about 690 and 650 MeV at 5.02A and 2.76A TeV, respectively, at time τ_0. We see that the average temperature is significantly larger at the FCC compared with the LHC energies throughout the evolution of the fireball. A sharp fall in $\langle T \rangle$ is observed for $\tau < 4$ fm/c for all three energies. However, the much larger value of $\langle T \rangle$ even after 4 fm time period at the FCC implies that the QGP phase is longer lived at the FCC than at the LHC. The average lifetime of the QGP phase obtained from the $\langle T \rangle$ vs τ curve is about 9.3, 7.6, and 7.1 fm at energies 39A, 5.02A, and 2.76A TeV, respectively. The rise in $\langle v_T \rangle$ with τ is found to

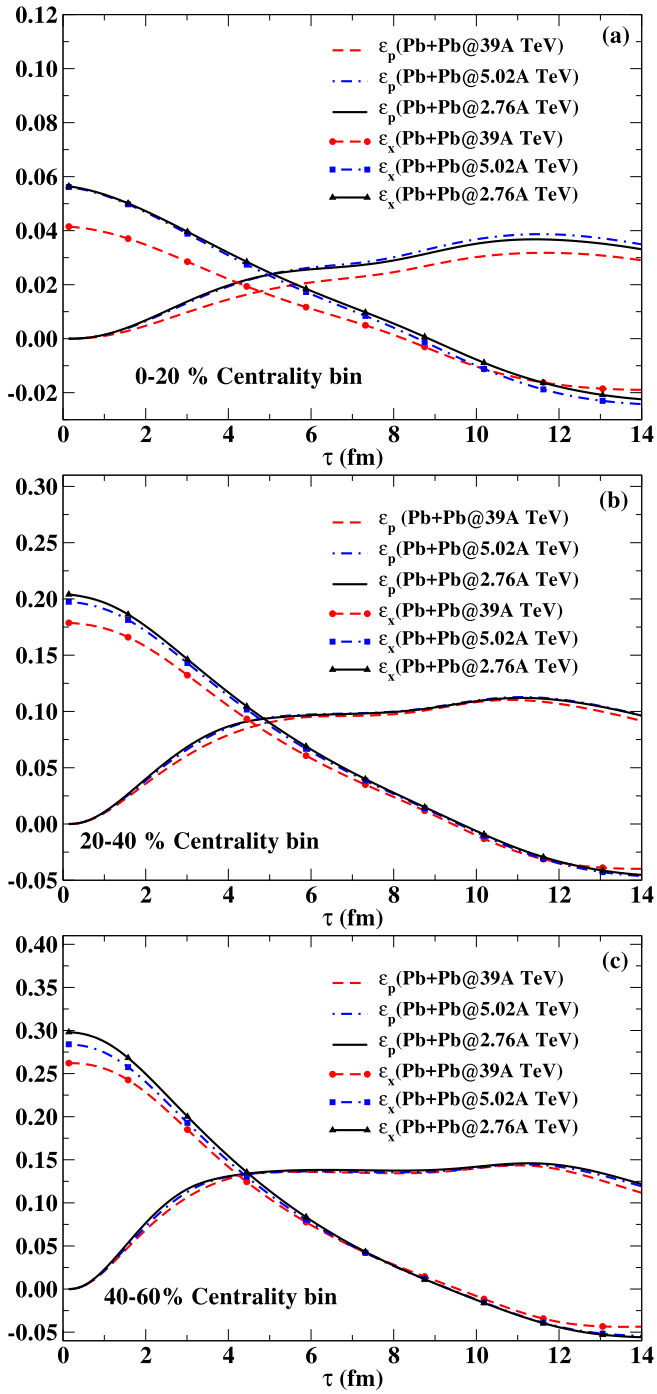

FIG. 4. Time evolution of spatial and momentum anisotropies in Pb + Pb collisions at 2.76A and 5.02A TeV at the LHC and at 39A TeV at the FCC for centrality bins (a) 0%–20%, (b) 20%–40%, and (c) 40%–60%.

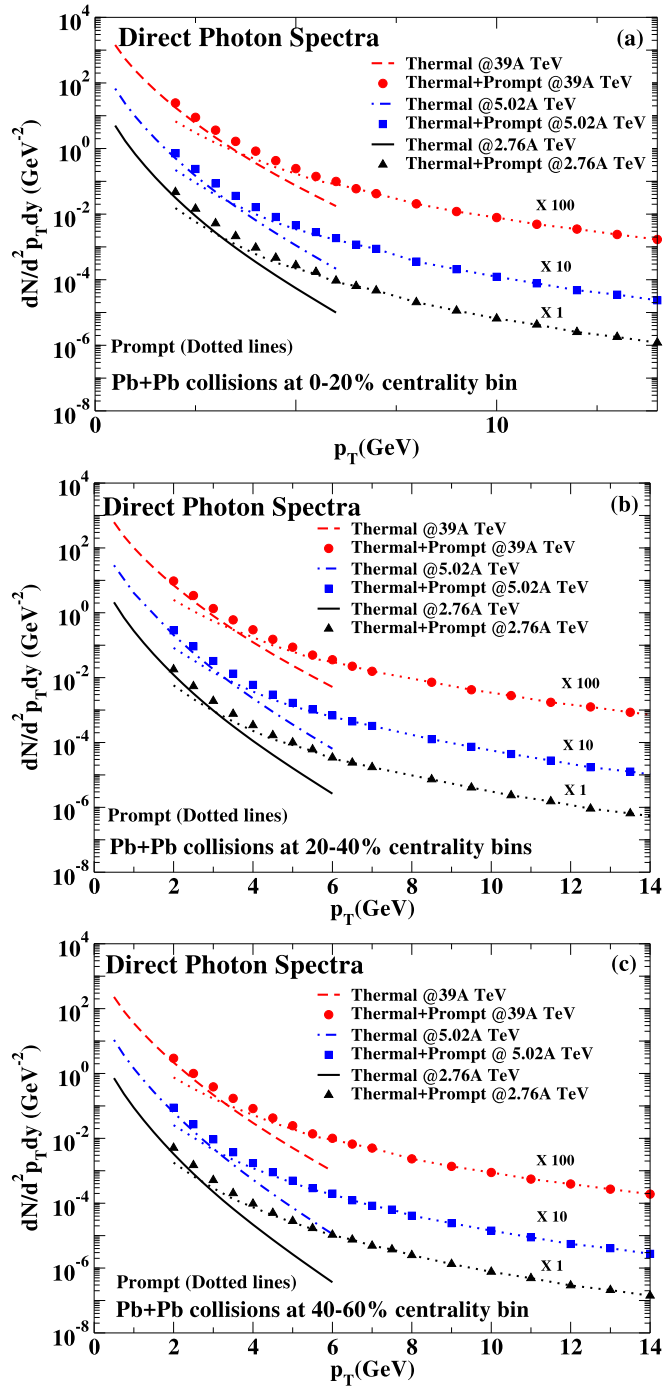

FIG. 5. Thermal- and (thermal + prompt)-photon spectra from Pb + Pb collisions at 2.76A and 5.02A TeV at the LHC and the FCC at 39A TeV for centrality bins (a) 0%–20%, (b) 20%–40%, and (c) 40%–60%.

be similar in the first 2–3 fm/c time period for FCC and LHC energies. However, for $\tau >$ 4 fm/c the average transverse flow velocity rises at a faster rate at FCC energies than at LHC energies.

We show the time evolution of the spatial (ϵ_x) and momentum (ϵ_p) anisotropies [calculated by using Eqs. (6) and (7), respectively, of Ref. [11]] at the three collision energies and for all three different centrality bins in Fig. 4. The spatial anisotropy is found to be a little large for the lowest beam energy at all three centrality bins. On the other hand, ϵ_p is found to be similar for all three centrality bins except for the 0%–20% central collisions where it is smallest for the FCC energy.

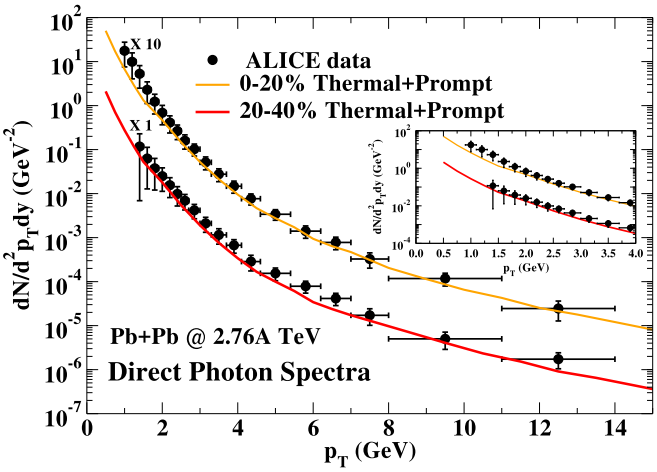

FIG. 6. Direct photon spectra for 0%–20% and 20%–40% centrality bins at 2.76A Pb + Pb collisions at the LHC along with ALICE data [18].

C. Direct photon production

The thermal-photon spectra from Pb + Pb collisions at FCC and LHC energies are shown in Fig. 5 for centrality bins 0%–20%, 20%–40%, and 40%–60%. The direct photon spectra obtained by adding the prompt and thermal photons together are also shown in the same figures for comparison. The photon spectra from our calculation are found to explain the ALICE direct photon data [18] for Pb + Pb collisions at 2.76A TeV well for 0%–20% and 20%–40% centrality bins, as shown in Fig. 6. The thermal radiation which dominates the direct photon spectrum up to 3–4 GeV increases significantly at FCC compared with LHC energies. At $p_T \sim 1$ GeV, the photon spectra at 5.02A TeV are found to be almost 1.5 times larger compared with the results at 2.76A TeV whereas, at FCC energies, those are almost 3.5 times larger than at 2.76A TeV at the same p_T value. Note that a smaller value (than 0.14 fm) of formation time τ_0 at 5.02A and 39A TeV would increase the thermal-photon production even more than the results shown in this study.

To understand the relative contributions of the prompt and thermal photons at different beam energies and p_T bins, we plot their ratio as a function of p_T in Fig. 7. One can see that the ratio is <1 at $p_T \sim 2.0$ GeV and then rises for higher p_T values. The radiations from thermal medium and initial hard scatterings become equal at $p_T \sim 3.5$ GeV at FCC energies and around $p_T \sim 3.0$ GeV at both LHC energies for most-central Pb + Pb collisions. The prompt contribution starts dominating over the thermal radiation as we move towards higher p_T values and the value of the ratio increases much more rapidly. For $p_T > 5$ GeV the prompt photons completely outshine the thermal radiation and, at this p_T, the ratio is much larger than unity for all three energies. Thus, we conclude that the relative enhancement in thermal-photon production compared with the prompt photons is larger at FCC energies in comparison to the LHC energies. In other words, the thermal radiation dominates the direct photon spectra up to a larger p_T value at FCC energies than at LHC energies.

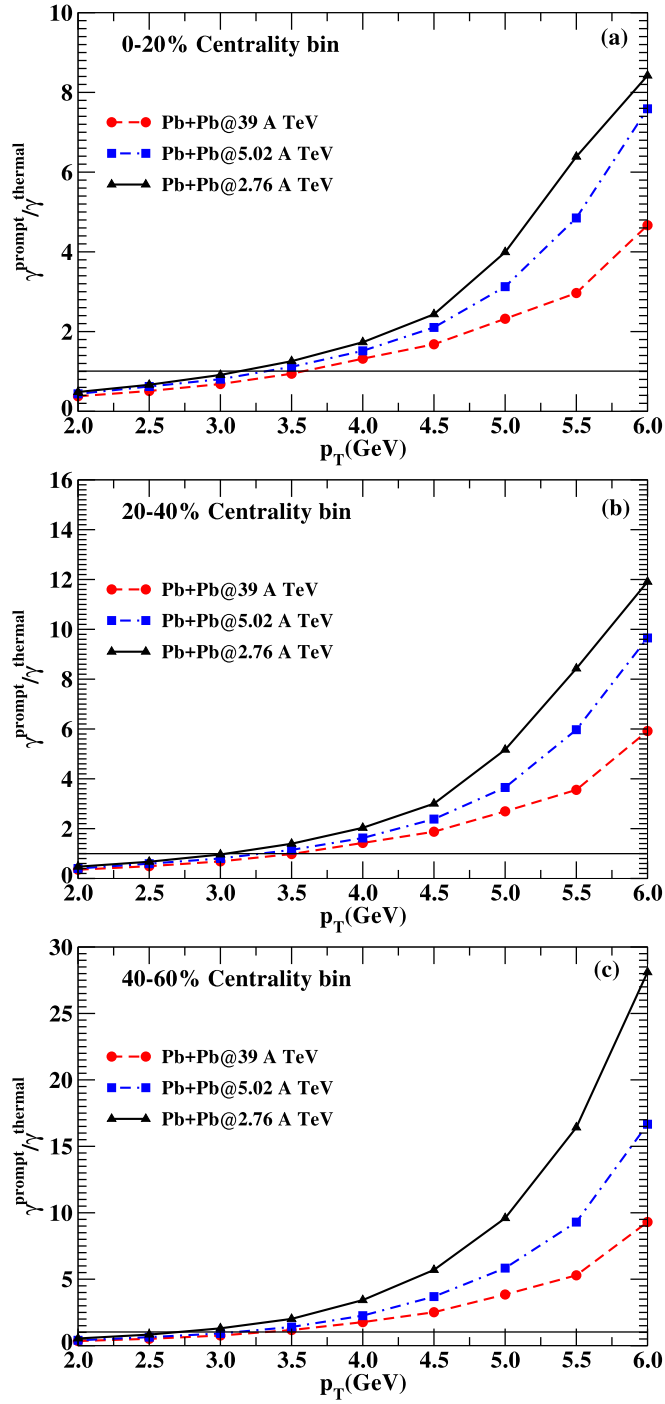

FIG. 7. Ratio of prompt- and thermal-photon production from Pb + Pb collisions at 2.76A and 5.02A TeV at the LHC and the FCC at 39A TeV for centrality bins (a) 0% –20%, (b) 20%–40%, and (c) 40%–60%.

The photon elliptic flow parameter v_2 as a function of p_T is shown in Fig. 8. For 0%–20% central collisions the thermal photon v_2 for all three energies are found to be small and close to each other. We see the photon v_2 at FCC energies is slightly smaller for $p_T < 2.5$ GeV than the elliptic flow calculated at the two LHC energies. As we move toward peripheral collisions, the thermal photon v_2 is found to be larger for the

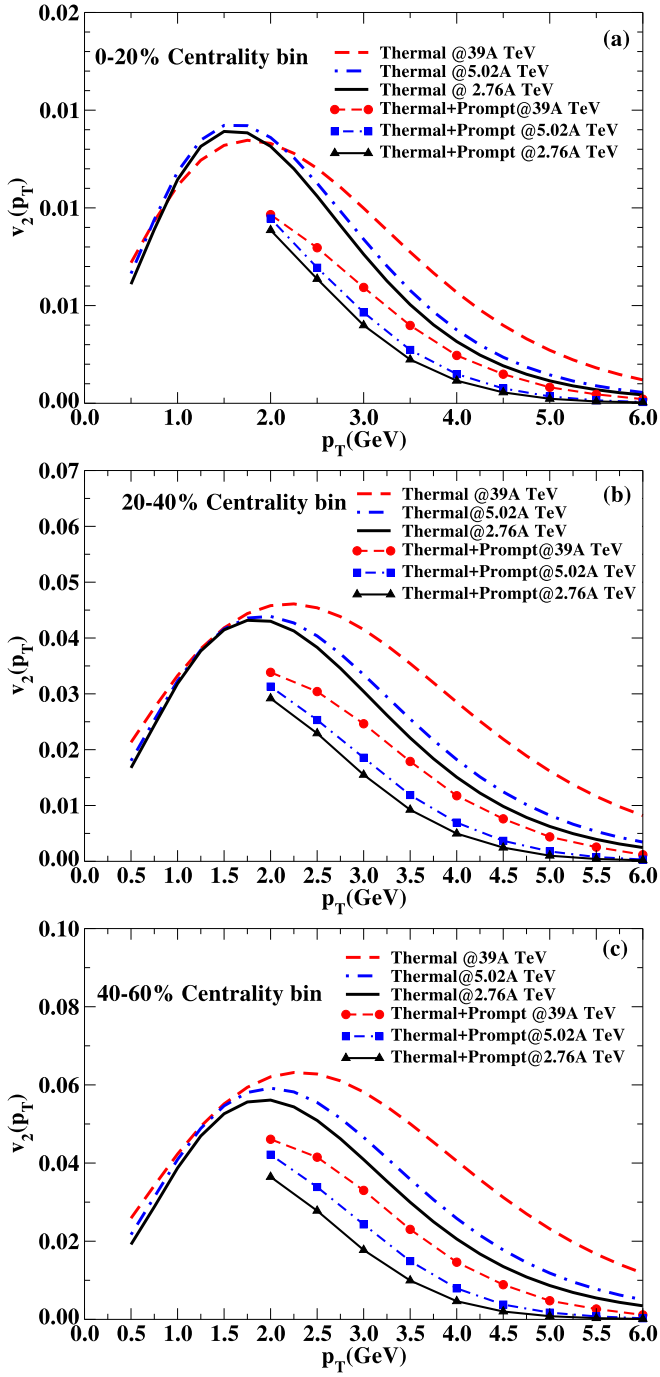

FIG. 8. Thermal photon and direct (thermal + prompt) photon v_2 from Pb + Pb collisions at 2.76A and 5.02A TeV at the LHC and at 39A TeV at the FCC for centrality bins (a) 0%–20%, (b) 20%–40%, and (c) 40%–60%.

higher beam energies. The difference between the v_2 values (as a function of p_T) at the three energies increases as we go to more peripheral collisions. The prompt photons produced in these collision do not contribute directly to the photon v_2; however, they dilute the thermal v_2 by adding extra weight at the denominator of the photon v_2 calculation [see Eq. (9) of Ref. [11]]. The direct photon v_2 is also plotted in Fig. 8 for comparison. We see a significant decrease in the elliptic flow for direct photons at all three energies compared with the thermal photon v_2.

VI. SUMMARY AND CONCLUSIONS

We predict the direct photon transverse momentum spectra from Pb + Pb collisions at 5.02A TeV at the LHC and at 39A TeV at the proposed Future Circular Collider Facility at CERN. The prompt-photon production is estimated by using a NLO perturbative QCD Monte Carlo code JETPHOX where the scales of factorization, renormalization, and fragmentation are set equal to p_T of the photon. We have used the CTEQ6.6 parton distribution function, the BFG-II parton-to-photon fragmentation function, and EPS09 parametrization of the nuclear shadowing function in this work. Thermal photon spectra and elliptic flow are calculated by using a (2 + 1)-dimensional longitudinally boost-invariant ideal hydrodynamic framework and state-of-the-art photon rates. The prompt-photon production is found to be significantly enhanced in Pb + Pb collisions at 39A TeV in comparison to 5.02A and 2.76A TeV for all three centrality bins. The enhancement factor ranges from 5 to 15 in the p_T region of 2 to 15 GeV. The time evolution of average transverse flow velocity and average temperature is also found to be significantly larger at 39A TeV compared with the two LHC energies. However, the spatial anisotropy ϵ_x as a function of τ is found to be smaller for 39A TeV than at 5.02 and 2.76A TeV. The momentum anisotropy parameter ϵ_p is found to be slightly smaller for 39A TeV; otherwise, it is close to each other for all three energies.

The thermal photon production is found to be enhanced by a large factor for Pb + Pb collisions at 39A TeV compared with 5.02A and 2.76A TeV. However, we notice that the relative enhancement in prompt-photon production compared with thermal photons is more in peripheral collisions for all beam energies. For example, the prompt-to-thermal-photon ratio is ∼10 at $p_T = 6$ GeV for 40%–60% Pb + Pb collisions at FCC whereas, the ratio is close to four for 0%–20% centrality bin. The direct (thermal + prompt) photon transverse momentum spectra for Pb + Pb collisions at 2.76A TeV from our calculation are found to explain the ALICE experimental data well in the region $p_T > 2$ GeV. The v_2 of thermal photons at FCC energies is found to be slightly larger than the v_2 at the other two LHC energies in the region $p_T > 2$ GeV. The direct photon v_2 is estimated by adding the prompt contribution to the photon yield, and we see that the elliptic flow of photons decreases significantly in the high-p_T region. The direct photon elliptic flow at different beam energies presented here might not explain the experimental data; however, it shows the sensitivity of photon v_2 to the collision energies which is the primary focus of the current study. We have seen that the thermal- and prompt-photon production and the elliptic flow of the thermal photons change at a differing rates as the energy (and the resulting initial conditions) of the collision increases. Thus, a simultaneous description of the direct photon spectra and their elliptic flow will put strong constraints on a theoretical description. This should prove to be quite valuable.

ACKNOWLEDGMENTS

We thank the Computer and Informatics group VECC for providing computer facility. P.D. is grateful to Department of Atomic Energy, Government of India for financial support. S.D. gratefully acknowledges the hospitality provided by VECC during his visit. D.K.S. gratefully acknowledges the grant of a Raja Ramanna Fellowship by the Department of Atomic Energy, India and support from the ExtreMe Matter Institute EMMI at the GSI Helmholtzzentrum für Schwerionenforschung, Darmstadt, Germany.

[1] J. W. Harris and B. Muller, Annu. Rev. Nucl. Part. Sci. **46**, 71 (1996).
[2] E. Shuryak, Rev. Mod. Phys. **89**, 035001 (2017).
[3] P. Kolb and U. Heinz, *Quark Gluon Plasma 3*, edited by R. C. Hwa *et al.* (World Scientific, Singapore, 2003), p. 634.
[4] K. J. Eskola, H. Honkanen, H. Niemi, P. V. Ruuskanen, and S. S. Rasanen, Phys. Rev. C **72**, 044904 (2005); Ann. Rev. Nucl. Part. Sci. **56**, 163 (2006).
[5] P. Huovinen, P. Kolb, U. Heinz, P. V. Ruuskanen, and S. Voloshin, Phys. Lett. B **503**, 58 (2001).
[6] D. Teaney, J. Lauret, and E. V. Shuryak, Phys. Rev. Lett. **86**, 4783 (2001).
[7] Z. Qiu, C. Shen, and U. Heinz, Phys. Lett. B **707**, 151 (2012).
[8] H. Petersen, R. L. Placa, and S. A. Bass, J. Phys. G **39**, 055102 (2012).
[9] P. V. Ruuskanen, Nucl. Phys. A **544**, 169 (1992), and references therein.
[10] D. K. Srivastava, J. Phys. G **35**, 104026 (2008).
[11] R. Chatterjee, H. Holopainen, I. Helenius, T. Renk, and K. J. Eskola, Phys. Rev. C **88**, 034901 (2013).
[12] R. Chatterjee, D. K. Srivastava, and T. Renk, Phys. Rev. C **94**, 014903 (2016).
[13] J. F. Paquet, C. Shen, G. S. Denicol, M. Luzum, B. Schenke, S. Jeon, and C. Gale, Phys. Rev. C **93**, 044906 (2016).
[14] O. Linnyk, V. P. Konchakovski, W. Cassing, and E. L. Bratkovskaya, Phys. Rev. C **88**, 034904 (2013).
[15] R. Chatterjee, P. Dasgupta, and D. K. Srivastava, Phys. Rev. C **96**, 014911 (2017).
[16] A. Adare *et al.* (PHENIX Collaboration), Phys. Rev. Lett. **104**, 132301 (2010); Phys. Rev. C **91**, 064904 (2015).
[17] A. Adare *et al.* (PHENIX Collaboration), Phys. Rev. Lett. **109**, 122302 (2012); Phys. Rev. C **94**, 064901 (2016).
[18] M. Wilde (ALICE Collaboration), Nucl. Phys. A **904-905**, 573c (2013); J. Adam *et al.* (ALICE Collaboration), Phys. Lett. B **754**, 235 (2016).
[19] D. Lohner and for the ALICE Collaboration, J. Phys.: Conf. Ser. **446**, 012028 (2013).
[20] P. Dasgupta, R. Chatterjee, and D. K. Srivastava, Phys. Rev. C **95**, 064907 (2017).
[21] P. Dasgupta, R. Chatterjee, S. K. Singh, and Jan-e Alam, Phys. Rev. C **97**, 034902 (2018).
[22] H. Holopainen, S. S. Rasanen, and K. J. Eskola, Phys. Rev. C **84**, 064903 (2011).
[23] H. V. Hees, M. He, and R. Rapp, Nucl. Phys. A **933**, 256 (2015).
[24] K. Dusling, Nucl. Phys. A **839**, 70 (2010).
[25] M. Dion, J.-F. Paquet, B. Schenke, C. Young, S. Jeon, and C. Gale, Phys. Rev. C **84**, 064901 (2011).
[26] C. Shen, U. W. Heinz, J.-F. Paquet, and C. Gale, Phys. Rev. C **89**, 044910 (2014); **91**, 024908 (2015).
[27] H. van Hees, C. Gale, and R. Rapp, Phys. Rev. C **84**, 054906 (2011).
[28] O. Linnyk, W. Cassing, and E. L. Bratkovskaya, Phys. Rev. C **89**, 034908 (2014).
[29] F.-M. Liu and S.-X. Liu, Phys. Rev. C **89**, 034906 (2014).
[30] C. Gale, Y. Hidaka, S Jeon, S. Lin, J.-F. Paquet, R. D. Pisarski, D. Satow, V. V. Skokov, and G. Vujanovic, Phys. Rev. Lett. **114**, 072301 (2015).
[31] A. Monnai, Phys. Rev. C **90**, 021901 (2014).
[32] L. McLerran and B. Schenke, Nucl. Phys. A **929**, 71 (2014); **946**, 158 (2016).
[33] V. Vovchenko, Iu. A. Karpenko, M. I. Gorenstein, L. M. Satarov, I. N. Mishustin, B. Kampfer, and H. Stoecker, Phys. Rev. C **94**, 024906 (2016).
[34] J. Berges, K. Reygers, N. Tanji, and R. Venugopalan, Phys. Rev. C **95**, 054904 (2017); Nucl. Phys. A **967**, 708 (2017).
[35] S. A. Bass, B. Muller, and D. K. Srivastava, Phys. Rev. Lett. **90**, 082301 (2003).
[36] M. Greif, F. Senzel, H. Kremer, K. Zhou, C. Greiner, and Z. Xu, Phys. Rev. C **95**, 054903 (2017).
[37] L. Oliva, M. Ruggieri, S. Plumari, F. Scardina, G. X. Peng, and V. Greco, Phys. Rev. C **96**, 014914 (2017).
[38] S. Caron-Huot, P. Kovtun, and G. D. Moore, J. High Energy Phys. 12 (2006) 015.
[39] B. Muller, S.-Y. Wu, and D.-L. Yang, Phys. Rev. D **89**, 026013 (2014).
[40] I. Iatrakis, E. Kiritsis, C. Shen, and D.-L. Yang, J. High Energy Phys. 04 (2017) 035.
[41] R. Chatterjee and D. K. Srivastava, Phys. Rev. C **79**, 021901(R) (2009); Nucl. Phys. A **830**, 503c (2009).
[42] R. Chatterjee, H. Holopainen, T. Renk, and K. J. Eskola, Phys. Rev. C **85**, 064910 (2012); arXiv:1207.6917.
[43] CERN FCC web site, http://www.fcc.web.cern.ch.
[44] N. Armesto, A. Dainese, D. d'Enterria, S. Masciocchi, C. Roland, C. Salgado, M. van Leeuwen, and U. Wiedemann, Nucl. Phys. A **931**, 1163 (2014).
[45] A. Dainese *et al.*, arXiv:1605.01389; N. Armesto *et al.*, Nucl. Phys. A **956**, 854 (2016).
[46] F. Arleo *et al.*, arXiv:hep-ph/0311131.
[47] J. C. Collins, D. E. Soper, and G. Sterman, Nucl. Phys. B **261**, 104 (1985).
[48] R. D. Field, *Applications of Perturbative QCD* (Addison-Wesley Publishing Company, Reading, MA, 1989).
[49] D. F. Geesaman, K. Saito, and A. W. Thomas, Annu. Rev. Nucl. Part. Sci. **45**, 337 (1995).
[50] K. J. Eskola, H. Paukkunen, and C. A. Salgado, J. High Energy Phys. 04 (2009) 065.
[51] R. Chatterjee, D. K. Srivastava, and S. Jeon, Phys. Rev. C **79**, 034906 (2009).
[52] P. M. Nadolsky, H.-L. Lai, Q.-H. Cao, J. Huston, J. Pumplin, D. Stump, W.-K. Tung, and C.-P. Yuan, Phys. Rev. D **78**, 013004 (2008).

[53] L. Bourhis, M. Fontannaz, and J. P. Guillet, Eur. Phys. J. C **2**, 529 (1998).
[54] P. Aurenche, J. P. Guillet, E. Pilon, M. Werlen, and M. Fontannaz, Phys. Rev. D **73**, 094007 (2006).
[55] J. F. Owens, Rev. Mod. Phys. **59**, 465 (1987).
[56] S. De and D. K. Srivastava, J. Phys. G **39**, 015001 (2012).
[57] S. De, J. Phys. G **44**, 045104 (2017).
[58] H. Holopainen, H. Niemi, and K. J. Eskola, Phys. Rev. C **83**, 034901 (2011).
[59] R. Chatterjee, H. Holopainen, T. Renk, and K. J. Eskola, Phys. Rev. C **83**, 054908 (2011); J. Phys. G. Nucl. Part. Phys. **38**, 124136 (2011).
[60] M. Laine and Y. Schroder, Phys. Rev. D **73**, 085009 (2006).
[61] P. Arnold, G. D. Moore, and L. G. Yaffe, J. High Energy Phys. 12 (2001) 009.
[62] J. Ghiglieri, J. Hong, A. Kurkela, E. Lu, G. D. Moore, and D. Teaney, J. High Energy Phys. 05 (2013) 010.
[63] S. Turbide, R. Rapp, and C. Gale, Phys. Rev. C **69**, 014903 (2004).